HHS Public Access

Author manuscript

Neuron. Author manuscript; available in PMC 2018 February 08.

Published in final edited form as:

Neuron. 2017 February 08; 93(3): 522–532.e5. doi:10.1016/j.neuron.2016.12.035.

Studying brain circuit function with dynamic causal modeling for optogenetic fMRI

David Bernal-Casas[1], **Hyun Joo Lee**[1], **Andrew J. Weitz**[1,2], and **Jin Hyung Lee**[1,2,3,4,*]

[1]Department of Neurology and Neurological Sciences, Stanford University, CA 94305, USA

[2]Department of Bioengineering, Stanford University, CA 94305, USA

[3]Department of Neurosurgery, Stanford University, CA 94305, USA

[4]Department of Electrical Engineering, Stanford University, Stanford, CA 94305, USA

Summary

Defining the large-scale behavior of brain circuits with cell type specificity is a major goal of neuroscience. However, neuronal circuit diagrams typically draw upon anatomical and electrophysiological measurements acquired in isolation. Consequently, a dynamic and cell type-specific connectivity map has never been constructed from simultaneous measurements across the brain. Here, we introduce dynamic causal modeling (DCM) for optogenetic fMRI experiments – which uniquely allow cell type-specific, brain-wide functional measurements – to parameterize the causal relationships among regions of a distributed brain network with cell type specificity. Strikingly, when applied to the brain-wide basal ganglia-thalamocortical network, DCM accurately reproduced the empirically observed time series, and the strongest connections were key connections of optogenetically stimulated pathways. We predict that quantitative and cell type-specific descriptions of dynamic connectivity, as illustrated here, will empower novel systems-level understanding of neuronal circuit dynamics and facilitate the design of more effective neuromodulation therapies.

Introduction

Many of the nervous system's key functions are orchestrated by large-scale distributed networks across the brain, including the basal ganglia-thalamocortical circuit, responsible for motor control. Therefore, to truly understand the circuit mechanism underlying motor control, the effective connectivity among multiple brain regions and neuronal populations must be defined. Effective connectivity is conventionally defined as the causal or directed coupling between brain regions, whereas functional connectivity refers to the correlations

*Corresponding author and lead contact: Jin Hyung Lee, PhD, ljinhy@stanford.edu, 1201 Welch Road, #P206, Stanford, CA 94305.

Author contributions: DBC designed and implemented the computational modeling approach and wrote the paper. HJL collected the ofMRI data. AJW processed the ofMRI data and helped write the paper. JHL designed and planned the overall study, supervised all personnel, and wrote the paper.

between them (Friston, 2011). Illuminating these causal relationships will facilitate a better understanding of neurological disease involving the basal ganglia, and allow for the optimization of therapies for movement disorders including deep brain stimulation (DBS) for Parkinson's disease.

Functional magnetic resonance imaging (fMRI) is an important tool that provides non-invasive measurements of neural activity across large-scale brain networks through surrogate hemodynamic responses like the blood oxygenation level dependent (BOLD) signal (Bandettini, 2012; Friston, 2009; Glover, 2011). Over the last several decades, significant progress has been made on understanding the relationship between neuronal activity and BOLD responses (Bandettini, 2014; Bandettini et al., 1992; Huettel et al., 2004; Huttunen et al., 2008; Kilner et al., 2005; Logothetis, 2008; Wang et al., 2012). However, normally, the measurements made with fMRI cannot be linked to specific cell types, complicating the interpretation of these studies. On the other hand, while advanced modeling approaches have been increasingly applied to study the functional interactions underlying brain-wide network activity measured with fMRI (Deco and Kringelbach, 2014; Friston et al., 2014b; Sporns, 2010), these too would be more powerful if combined with measurements that provide cell type-specific network function.

The basal ganglia-thalamocortical network motivates the importance of defining cell type-specific network function. The striatum – the primary input structure of the basal ganglia – has distinct cell types including D1- and D2-receptor-expressing medium spiny neurons (D1- and D2-MSNs), which send unique inhibitory projections to surrounding basal ganglia nuclei (Bertran-Gonzalez et al., 2010; Deng et al., 2006; Gerfen et al., 1990). D1-MSNs project directly to the two output nuclei of the basal ganglia – the internal globus pallidus and the substantia nigra pars reticulata – and are thought to promote motor behavior via disinhibition of downstream thalamocortical circuits, while D2-MSNs project indirectly to the two output nuclei via the external globus pallidus and subthalamic nucleus, and are thought to inhibit movement by suppressing thalamocortical circuits (Albin et al., 1989; DeLong, 1990; Kravitz et al., 2010). Because different cell types have clear, distinct functions, it is critical that experimental measurements of motor control by this network be performed with cell type specificity.

Optogenetic fMRI (ofMRI) now uniquely enables monitoring of brain-wide functional activity resulting from cell type-specific perturbations (Abe et al., 2012; Desai et al., 2011; Duffy et al., 2015; Gerits et al., 2012; Kahn et al., 2013; Lee et al., 2010; Liu et al., 2015; Ohayon et al., 2013; Weitz et al., 2015; Weitz and Lee, 2013). Recently, we used this platform to characterize the opposing patterns of activity across the basal ganglia-thalamocortical network upon selective stimulation of either D1- or D2-MSNs (Lee et al., 2016). Importantly, we precisely traced temporal signal patterns across the brain and found that they generally matched the underlying single-unit electrophysiology (Lee et al., 2016). However, given the multi-dimensional nature of the data and the high degree of connectivity across brain regions, it was impossible to infer causal influences among different regions by observation alone. Furthermore, complex downstream effects may also contribute to brain-wide network dynamics and complicate interpretations. To overcome this problem, here we applied dynamic causal modeling (DCM) to parameterize these causal relationships.

DCM is a Bayesian procedure that allows one to estimate coupling (effective connectivity) and evidence for different network models of neuroimaging data (Friston et al., 2003). A wide variety of models have been proposed, ranging from nonlinear models (Stephan et al., 2008) to stochastic approaches (Li et al., 2011) and spectral formulations (Friston et al., 2014a). In stochastic DCM, both the effective connectivity and endogenous (neuronal) fluctuations are estimated. Importantly, stochastic DCM has been subject to neurobiological validation using simultaneous EEG-fMRI recordings (Daunizeau et al., 2012) and has been shown to offer high reproducibility in a multicenter study (Bernal-Casas et al., 2013). However, stochastic DCM is computationally very intensive. In contrast, spectral DCM (spDCM) parameterizes endogenous fluctuations and adapts a deterministic model of neuronal activity, which leads to significant increase in computation speed. Its validity has also been examined in relation to the biophysically validated stochastic DCM (Razi et al., 2015). In this study, we used spectral DCM to investigate the interactions among basal ganglia-thalamocortical network regions with cell type specificity and link the observed activation patterns to quantitative parameters that represent effective connectivity strengths. We also discuss implications of this dynamic causal modeling approach for revealing functional relationships underpinning brain-wide networks with cell type specificity beyond the basal ganglia.

Results

Dynamic causal modeling of ofMRI data

In order to computationally model the D1- and D2-MSN stimulation ofMRI data and identify effective connective strengths, we implemented spectral DCM. For fMRI, DCMs can either be fitted to the time series directly (standard DCM) - or to the cross spectral density of the data after applying a Fourier transform (spectral DCM). Both standard and spectral DCM can also include endogenous fluctuations beyond experimental effects. Although experimental effects and endogenous fluctuations are normally not considered together, our fMRI time series were elicited under optogenetically controlled experimental stimuli (i.e., a deterministic input), giving us the opportunity to compare deterministic and stochastic models of the same data and to ask whether stochastic endogenous fluctuations were necessary for explaining our data. We therefore performed Bayesian model comparison using spectral DCM with and without endogenous fluctuations. To quantify the quality of fit of the spectral DCM, we used the posterior estimates from the spectral DCM as priors in a standard (stochastic) DCM and reinverted the time series. This provided predicted responses in the time domain that were then compared to the observed signal. We selected a network model to use as the *a priori* generative model based on known basal ganglia anatomy. Based on recent publications (Calabresi et al., 2014; Schroll and Hamker, 2013), we implemented a seven-node brain network including the caudate-putamen (CPu), external globus pallidus (GPe), internal globus pallidus (GPi), subthalamic nucleus (STN), substantia nigra (SN), thalamus (THL), and motor cortex (MCX). We also modeled an alternative network defined by the replacement of motor cortex with sensory cortex (SCX) to examine the network's stability – defined here as the stability of connectivity estimates upon perturbations to the network.

We defined anatomical regions of interest for each node and extracted voxel-averaged fMRI time series (Figure 1). Figure 2 depicts the *a priori* connection scheme of the generative model employed throughout the study. Connectivity estimates were computed after low-pass filtering the time series with ten different cutoff frequencies, and the significance of each connection was determined at each cutoff by testing its connectivity estimate against zero across subjects (D1: $n = 12$, D2: $n = 10$). We then used false discovery rate (FDR) to correct the resulting p-values for multiple tests of network connections (at the between-subject level). Significant variability in the p-values was observed across cutoff frequencies (Figure S1). For the model's final output, we selected the filter cutoff that maximized a weighted sum of the number of significant and close-to-significant connections. Connections with a corrected p-value less than 0.05 were considered significant, while those having a corrected p-value between 0.05 and 0.10 were considered close-to-significant. The same criteria were applied for statistical significance when comparing connections under D1- and D2-MSN stimulations, and MCX and SCX networks.

To model endogenous fluctuations and observation noise parameters within the model, we used autoregressive models of order one to four, parameterized by amplitude and autoregressive model coefficients. As described above, we also investigated the importance of endogenous fluctuations in each network by comparing results with and without endogenous fluctuations in the model equations for stochastic and deterministic modeling, respectively. In particular, random effects Bayesian model selection (BMS) was used to select which of the two modeling approaches provided the greatest model evidence – in other words, the best balance between accuracy and complexity – and to examine the optimal order of autoregressive processes (Penny et al., 2004; Stephan et al., 2009). Full mathematical details can be found in the STAR Methods section.

Throughout this study, we utilize the DCM framework introduced by Friston (2003). Novelties in our approach include autoregressive modeling, a comparison of models with and without endogenous fluctuations, and the optimized selection of a low-pass filter cutoff frequency.

D1- and D2-MSN stimulation networks

Significant connections during D1-MSN stimulations were largely consistent with direct pathway activation (Figure 3A,D). Mean connectivity estimates with 95% confidence intervals across subjects and uncorrected and corrected p-values are provided in Table S1. Remarkably, the projections exhibiting the strongest connectivity estimates in both MCX and SCX networks were those from CPu to GPi (mean connectivity estimate: 0.9177 Hz, p-value (corrected): 0.0072, in the MCX network) and from CPu to SN (mean connectivity estimate: 0.9155 Hz, p-value (corrected): 3.6572×10^{-5}, in the MCX network) – the two defining connections of the direct pathway. Upon using the posterior estimates from the spectral DCM as priors in a standard (stochastic) DCM, the resulting time series reproduced the amplitude, polarities, and delays of the empirically observed BOLD responses across brain regions for both MCX and SCX network models (Figure 3B,E). In general, stochastic models (with endogenous fluctuations) were better than deterministic models. For the MCX network, the exceedance probability of stochastic modeling (i.e., the probability that this

modeling approach was more likely than any other modeling approach considered) was 0.9148 (Figure 3C). For the SCX network, the model exceedance probability of stochastic modeling was 0.5918 (Figure 3F).

The brain-wide fMRI responses to D2-MSN stimulation significantly differed from those evoked by D1-MSN stimulation. In particular, many of the subcortical regions exhibited a decrease in signal during stimulation. Importantly, using the same *a priori* network described above now led to significant connections that reflected activation of the indirect pathway (Figure 4A,D). Mean connectivity coefficients with 95% confidence intervals across subjects and uncorrected and corrected p-values are shown in Table S2. The greatest connection in both MCX and SCX network models was from GPe to STN (mean connectivity estimate: 1.1176 Hz, p-value (corrected): 5.7809×10^{-4}, in the MCX network) – a key projection of the indirect pathway. The time series calculated from these posterior estimates also accurately matched the distinct BOLD responses elicited by D2-MSN stimulation, such as the robust negative signal within the thalamus (Figure 4B,E). As with D1-MSN stimulations, stochastic models were better than deterministic models in a majority of subjects. The exceedance probability of stochastic modeling was 0.6025 for the MCX network (Figure 4C) and 0.7529 for the SCX network (Figure 4F).

In light of the close relationship between model estimates and underlying physiology, it should again be emphasized that the same modeling framework was used to estimate networks during D1- and D2-MSN stimulations. The generative model, fluctuations, and priors remained the same. This demonstrates that the proposed algorithm can be generalized for use in parameterizing different optogenetic fMRI experiments.

Comparison between MCX and SCX network models

We next examined the stability of D1-MSN-driven networks. The exchange of MCX with SCX did not change the strength of any connection within the model (Figure 5A, Table S3), supporting the idea that motor and sensory cortices generally exert homologous influence on basal ganglia circuitry during D1-MSN stimulations. Similarly, the replacement of motor cortex with sensory cortex for the D2-MSN stimulation models did not significantly change the strength of inter-regional connectivity estimates (Figure 5B, Table S3). Only the self-connection within cortex was different in strength after replacement (close-to-significant, $P < 0.10$). Collectively, these results demonstrate the stability of dynamic causal modeling in D1- and D2-MSN stimulation networks.

Comparison between D1- and D2-MSN stimulation network models

To provide a quantitative comparison of the D1- and D2-MSN stimulation network models, we performed statistical comparisons of each model's resulting connectivity estimates (Figure 6, Table S4). Connections from CPu to GPi and from CPu to SN – the defining projections of the direct pathway – were significantly greater during D1-MSN stimulations in both MCX and SCX networks. The connection from STN to SN – another key projection within the indirect pathway – was greater during D2-MSN stimulations in the SCX network (close-to-significant, $P < 0.10$). We also observed differences in the strength of cortical efferents between the D1- and D2-MSN stimulations. On the other hand, the connection

from MCX to THL was significantly greater during D1-MSN stimulations. These projections were generally positive during D1-MSN stimulation, and negative during D2-MSN stimulations.

There were also several significant differences in intra-regional estimates between D1- and D2-MSN stimulations (Table S4). The self-connection parameters within the CPu were significantly greater in magnitude (more negative) during D1-MSN stimulations in both MCX and SCX networks. In the GPe, the self-connection parameter was significantly greater in magnitude (more negative) during D2-MSN stimulations in the MCX network. The self-connection parameters in GPi were also greater in magnitude (more negative) during D2-MSN stimulations in the SCX network (close-to-significant, $P < 0.10$). Likewise, the self-connection parameter in STN was greater in magnitude (more negative) during D2-MSN stimulations in the MCX network (close-to-significant, $P < 0.10$). The self-connection parameters within SN were significantly greater in magnitude (more negative) during D2-MSN stimulations in both MCX and SCX networks. Finally, in the SCX network, the self-connection parameter in SCX was significantly greater in magnitude (more negative) during D2-MSN stimulations.

Discussion

While circuit diagrams of basal ganglia pathways have been traditionally delineated by measuring anatomical connectivity and electrophysiological activity in isolation, they have never been simultaneously and directly measured across the brain. Our model makes use of brain-wide optogenetic fMRI measurements to construct the first cell type-specific dynamic brain circuit diagram based on data measured in live subjects. In this study, we developed a computational approach that can parameterize the brain-wide network function measured by fMRI responses evoked during cell type-specific stimulations of D1- or D2-receptor-expressing striatal MSNs. Strikingly, the strongest connections during D1-MSN stimulation were the efferents from the CPu to GPi and SN, while the strongest connection during D2-MSN stimulation was from GPe to STN – the key projections of the direct and indirect pathways, respectively. Comparisons of connectivity estimates between the two stimulation groups also revealed that connections belonging to the direct pathway were greater during D1-MSN stimulation, and connections belonging to the indirect pathway were greater during D2-MSN stimulation. These findings confirm our method's ability to detect selective changes in effective connectivity within a distributed network under cell type-specific interventions, and underscore how effective connectivities among regions may depend on the cell types activated. Formally, this paper offers a construct validation of optogenetic fMRI DCM by appealing to the known functional anatomy and synaptic circuitry of the basal ganglia-thalamocortical system.

We found that stochastic models were better than deterministic models across networks and stimulation groups. The greater model evidence exhibited by the stochastic models suggests that there are neuronal processes that cannot be explained strictly by the experimental stimulus. Stochastic modeling, which accounts for endogenous fluctuations, may therefore be optimal for future modeling studies and offer greater generalization across experiments, as it provides the best balance between accuracy and complexity for explaining the measured

data (i.e., the greatest model evidence) (Figure S2 A-D). The optimal degree of complexity for these endogenous fluctuations was also examined by fitting autoregressive models of increasing order. Our results indicate that a relatively low order of local temporal correlations (e.g., *AR(1)* or *AR(2)* processes) was optimal across networks and stimulation groups (Figure S2 E-H).

Replacement of the motor cortex with sensory cortex revealed a stability of the connectivity parameters within the basal ganglia-thalamocortical circuit. No significant differences were observed in the strength of inter-regional connectivity estimates when replacing MCX by SCX (Table S3), and both network models yielded similar connections (Tables S1-2). This is a crucial property that must hold true in order for a causal estimation algorithm to be considered robust. It should be noted, however, that the selection of one model or the other did alter statistical effects across D1- and D2-MSN stimulations (Tables S1-2). For example, the connection from thalamus to cortex was not statistically significant in the SCX network model during D2-MSN stimulations, leaving no pathway from the stimulation site to cortex and thus compromising the interpretation of causality within the basal ganglia-thalamocortical system (Figure 4D). In this respect, the MCX network model may offer more mechanistic insight than the SCX network model, as it exhibited causality between regions across the overall system, including connections from thalamus to cortex and from cortex to striatum during both perturbations (Figures 3,4). Our failure to detect a causal relationship from thalamus to sensory cortex during D2-MSN stimulation suggests that thalamus may directly influence motor – but not sensory – cortex during D2-MSN stimulations. Notably, this did not prevent the accurate prediction of observed responses with either network model. This is possibly due to the inclusion of endogenous fluctuations in the model equations, which were able to account for hidden neuronal responses that were not explicitly included in the network models.

We also found that the signs of significant connections during D1- and D2-MSN stimulations were consistent with the diversity of temporal profiles and polarities of fMRI responses. During D1-MSN stimulations, for example, time series throughout the basal ganglia increased during stimulation. As expected, significant connectivity estimates throughout the basal ganglia-thalamocortical system were positive (Figure 3, Table S1). While the initial drop in sensory cortex may be seen as an exception to this, our proposed model interprets this transient as a reflection of a delay in cortical activations. During D2-MSN stimulations, connectivity estimates were positive all the way from CPu to cortex (Figure 4, Table S2). However, the BOLD responses – especially in thalamus – generally decreased during stimulation. The feedforward aspect of the indirect pathway therefore fails to explain the decreasing responses observed within STN, GPi, SN and thalamus. Nevertheless, this issue might be resolved once the signal passes through the cortex. As shown in Figure 4, the connection from cortex to STN was significantly negative, while the connections from STN to GPi, GPi to THL, STN to SN, and SN to THL were positive. Applying the multiplication operation along this pathway leads to a negative response within the STN, GPi, SN, and THL, and suggests that it may be the hyperdirect pathway, which is statistically significant and negative during D2-MSN stimulations, that explains the negative BOLD responses within these regions.

Beyond an understanding of normal basal ganglia information processing, our results offer insight into the mechanisms of movement disorders that originate from defects in this network. Optogenetically driving D2-MSNs, for example, simulates the loss of dopamine in striatum that is associated with Parkinson's disease (PD) by creating an imbalance in direct and indirect pathway activity. Interestingly, our connectivity analyses from D2-MSN stimulation revealed several features commonly observed in PD. First, we observed systematically more negative self-connection parameters within the basal ganglia's nuclei (STN, GPe, GPi, and SN) during D2-MSN stimulations compared to D1-MSN stimulations. Many of the self-connections exhibited a statistically significant or close-to-significant difference between D1- and D2-MSN stimulations for both the MCX and SCX network models (Table S4). Based on the mathematical solution of the state equation (see STAR Methods, Method Details), a more negative self-connection strength indicates that less time is needed to reach the activation state. One plausible interpretation of this is that brain regions within the basal ganglia synchronize faster during D2-MSN stimulation. Increased synchrony and neural oscillations in the STN and GPi have been observed in primate (Albin et al., 1989; Bergman et al., 1994; Nini et al., 1995) and rodent (Costa et al., 2006; Magill et al., 2001) models of PD. It has also been shown that STN activity correlates with downstream basal ganglia activity in PD monkeys (Deffains et al., 2016). Although the causal link between STN oscillations and PD symptoms remain elusive (Kuhn et al., 2009; Weinberger et al., 2009), it has been shown that pathological oscillations are suppressed by volitional movement (Amirnovin et al., 2004), dopamine replacement therapy (Brown et al., 2001; Levy et al., 2002; Priori et al., 2004; Weinberger et al., 2009), and STN-DBS therapy (Kuhn et al., 2008; Wingeier et al., 2006). As another possible link to PD, we observed statistically significant MCX-STN and close-to-significant SCX-STN connections during D2-, but not D1-MSN stimulations. Indeed, cortical-STN interactions have previously been implicated in PD mechanisms (Payoux et al., 2004; Ridding et al., 1995). It has even been suggested that the antiparkinsonian effects of STN stimulation result from selective activation of the M1-STN pathway (Gradinaru et al., 2009).

Neurostimulation therapy for PD aims at modulating neuronal activity of the basal ganglia-thalamocortical system. Clinically, the most common brain regions targeted to treat PD motor symptoms with DBS are the STN and GPi. While the exact mechanism of action for DBS in PD remains unclear, many hypotheses have been proposed (Chang et al., 2008; Hammond et al., 2008; McIntyre et al., 2004). For example, DBS may modulate abnormal synchronous oscillatory activity between the basal ganglia and cortical regions such as M1 (Walker et al., 2009; Whitmer et al., 2012). As a therapeutic alternative, recent data have suggested that epidural chronic motor cortex stimulation (MCS) could also improve symptoms resulting from movement disorders like PD (Priori and Lefaucheur, 2007). Among the possible mechanisms of action for MCS, it is hypothesized to reduce synchronized oscillatory activities in basal ganglia nuclei, similar to STN stimulation. We speculate that the connectivity analyses developed in this study can help elucidate the effectiveness of different regions as therapeutic targets. For example, the finding that motor cortex exhibits greater connectivity with subcortical structures during D2-MSN stimulation supports the hypothesis that motor cortex modulation may restore balance to Parkinsonian

circuitry and suggests that this region plays a critical role in the descending modulation of basal ganglia network activity.

It is worth noting that there were distinct, approximately orthogonal patterns of significant inter-regional connections between D1- and D2-MSN stimulations (Pearson's $r = -0.0363$ and -0.0368 for MCX and SCX network models, respectively). In distributed spatial representations, orthogonal arrangements of effective connectivity may be useful to maximize discriminability (Duncan, 2010). For example, they could be valuable in maintaining the separate identity and processing content of two populations with distinct cell types. In addition, orthogonal patterns can be employed to emit two independent sequences (e.g., a set of motor programs) simultaneously and to separate the received information afterwards (e.g., within the cerebral cortex).

In conclusion, these findings will open new research directions for characterizing functional brain systems. In future studies, causal influences among brain regions driven by a specific cell type can be quantified and compared in the healthy and diseased brain by utilizing optogenetic fMRI and the network models examined here. Knowing how neural pathways driven by specific cell populations contribute to diseases like PD will aid the development of treatments based on quantitative circuit mechanisms of disease, which will lead to improved targeted therapies with better efficacy and reduced adverse effects.

Supplementary Material

Refer to Web version on PubMed Central for supplementary material.

Acknowledgments

This work was supported by the NIH/NIBIB R00 Award (R00EB008738), Okawa Foundation Research Grant Award, NIH Director's New Innovator Award (DP2OD007265), the NSF CAREER Award (1056008), the Alfred P. Sloan Research Fellowship, and the NIH/NINDS R01 (R01NS091461).

References

Abe Y, Sekino M, Terazono Y, Ohsaki H, Fukazawa Y, Sakai S, Yawo H, Hisatsune T. Opto-fMRI analysis for exploring the neuronal connectivity of the hippocampal formation in rats. Neuroscience research. 2012; 74:248–255. [PubMed: 22982343]

Albin RL, Young AB, Penney JB. The functional anatomy of basal ganglia disorders. Trends in neurosciences. 1989; 12:366–375. [PubMed: 2479133]

Amirnovin R, Williams ZM, Cosgrove GR, Eskandar EN. Visually guided movements suppress subthalamic oscillations in Parkinson's disease patients. The Journal of neuroscience : the official journal of the Society for Neuroscience. 2004; 24:11302–11306. [PubMed: 15601936]

Bandettini PA. Twenty years of functional MRI: the science and the stories. Neuroimage. 2012; 62:575–588. [PubMed: 22542637]

Bandettini PA. Neuronal or hemodynamic? Grappling with the functional MRI signal. Brain connectivity. 2014; 4:487–498. [PubMed: 25093397]

Bandettini PA, Wong EC, Hinks RS, Tikofsky RS, Hyde JS. Time course EPI of human brain function during task activation. Magnetic resonance in medicine. 1992; 25:390–397. [PubMed: 1614324]

Bergman H, Wichmann T, Karmon B, DeLong MR. The primate subthalamic nucleus. II. Neuronal activity in the MPTP model of parkinsonism. Journal of neurophysiology. 1994; 72:507–520. [PubMed: 7983515]

Bernal-Casas D, Balaguer-Ballester E, Gerchen MF, Iglesias S, Walter H, Heinz A, Meyer-Lindenberg A, Stephan KE, Kirsch P. Multi-site reproducibility of prefrontal-hippocampal connectivity estimates by stochastic DCM. Neuroimage. 2013; 82:555–563. [PubMed: 23747286]

Bertran-Gonzalez J, Herve D, Girault JA, Valjent E. What is the Degree of Segregation between Striatonigral and Striatopallidal Projections? Frontiers in neuroanatomy. 2010; 4

Brown P, Oliviero A, Mazzone P, Insola A, Tonali P, Di Lazzaro V. Dopamine dependency of oscillations between subthalamic nucleus and pallidum in Parkinson's disease. The Journal of neuroscience : the official journal of the Society for Neuroscience. 2001; 21:1033–1038. [PubMed: 11157088]

Calabresi P, Picconi B, Tozzi A, Ghiglieri V, Di Filippo M. Direct and indirect pathways of basal ganglia: a critical reappraisal. Nature neuroscience. 2014; 17:1022–1030. [PubMed: 25065439]

Chang JY, Shi LH, Luo F, Zhang WM, Woodward DJ. Studies of the neural mechanisms of deep brain stimulation in rodent models of Parkinson's disease. Neuroscience and biobehavioral reviews. 2008; 32:352–366. [PubMed: 18035416]

Costa RM, Lin SC, Sotnikova TD, Cyr M, Gainetdinov RR, Caron MG, Nicolelis MA. Rapid alterations in corticostriatal ensemble coordination during acute dopamine-dependent motor dysfunction. Neuron. 2006; 52:359–369. [PubMed: 17046697]

Daunizeau J, Lemieux L, Vaudano AE, Friston KJ, Stephan KE. An electrophysiological validation of stochastic DCM for fMRI. Frontiers in computational neuroscience. 2012; 6:103. [PubMed: 23346055]

Deco G, Kringelbach ML. Great expectations: using whole-brain computational connectomics for understanding neuropsychiatric disorders. Neuron. 2014; 84:892–905. [PubMed: 25475184]

Deffains M, Iskhakova L, Katabi S, Haber SN, Israel Z, Bergman H. Subthalamic, not striatal, activity correlates with basal ganglia downstream activity in normal and parkinsonian monkeys. eLife. 2016; 5

DeLong MR. Primate models of movement disorders of basal ganglia origin. Trends in neurosciences. 1990; 13:281–285. [PubMed: 1695404]

Deng YP, Lei WL, Reiner A. Differential perikaryal localization in rats of D1 and D2 dopamine receptors on striatal projection neuron types identified by retrograde labeling. Journal of chemical neuroanatomy. 2006; 32:101–116. [PubMed: 16914290]

Desai M, Kahn I, Knoblich U, Bernstein J, Atallah H, Yang A, Kopell N, Buckner RL, Graybiel AM, Moore CI, et al. Mapping brain networks in awake mice using combined optical neural control and fMRI. Journal of neurophysiology. 2011; 105:1393–1405. [PubMed: 21160013]

Duffy BA, Choy M, Chuapoco MR, Madsen M, Lee JH. MRI compatible optrodes for simultaneous LFP and optogenetic fMRI investigation of seizure-like afterdischarges. Neuroimage. 2015; 123:173–184. [PubMed: 26208873]

Duncan J. The multiple-demand (MD) system of the primate brain: mental programs for intelligent behaviour. Trends in cognitive sciences. 2010; 14:172–179. [PubMed: 20171926]

Fang Z, Lee JH. High-throughput optogenetic functional magnetic resonance imaging with parallel computations. Journal of neuroscience methods. 2013; 218:184–195. [PubMed: 23747482]

Friston K, Mattout J, Trujillo-Barreto N, Ashburner J, Penny W. Variational free energy and the Laplace approximation. Neuroimage. 2007; 34:220–234. [PubMed: 17055746]

Friston KJ. Modalities, modes, and models in functional neuroimaging. Science. 2009; 326:399–403. [PubMed: 19833961]

Friston KJ. Functional and effective connectivity: a review. Brain connectivity. 2011; 1:13–36. [PubMed: 22432952]

Friston KJ, Harrison L, Penny W. Dynamic causal modelling. Neuroimage. 2003; 19:1273–1302. [PubMed: 12948688]

Friston KJ, Kahan J, Biswal B, Razi A. A DCM for resting state fMRI. Neuroimage. 2014a; 94:396–407. [PubMed: 24345387]

Friston KJ, Kahan J, Razi A, Stephan KE, Sporns O. On nodes and modes in resting state fMRI. Neuroimage. 2014b; 99:533–547. [PubMed: 24862075]

Gerfen CR, Engber TM, Mahan LC, Susel Z, Chase TN, Monsma FJ Jr. Sibley DR. D1 and D2 dopamine receptor-regulated gene expression of striatonigral and striatopallidal neurons. Science. 1990; 250:1429–1432. [PubMed: 2147780]

Gerits A, Farivar R, Rosen BR, Wald LL, Boyden ES, Vanduffel W. Optogenetically induced behavioral and functional network changes in primates. Current biology : CB. 2012; 22:1722–1726. [PubMed: 22840516]

Glover GH. Overview of functional magnetic resonance imaging. Neurosurgery clinics of North America. 2011; 22:133–139. vii. [PubMed: 21435566]

Glover GH, Lee AT. Motion artifacts in fMRI: comparison of 2DFT with PR and spiral scan methods. Magnetic resonance in medicine. 1995; 33:624–635. [PubMed: 7596266]

Gradinaru V, Mogri M, Thompson KR, Henderson JM, Deisseroth K. Optical deconstruction of parkinsonian neural circuitry. Science. 2009; 324:354–359. [PubMed: 19299587]

Hammond C, Ammari R, Bioulac B, Garcia L. Latest view on the mechanism of action of deep brain stimulation. Movement disorders : official journal of the Movement Disorder Society. 2008; 23:2111–2121. [PubMed: 18785230]

Huettel SA, McKeown MJ, Song AW, Hart S, Spencer DD, Allison T, McCarthy G. Linking hemodynamic and electrophysiological measures of brain activity: evidence from functional MRI and intracranial field potentials. Cerebral cortex. 2004; 14:165–173. [PubMed: 14704213]

Huttunen JK, Grohn O, Penttonen M. Coupling between simultaneously recorded BOLD response and neuronal activity in the rat somatosensory cortex. Neuroimage. 2008; 39:775–785. [PubMed: 17964186]

Jackson JI, Meyer CH, Nishimura DG, Macovski A. Selection of a convolution function for Fourier inversion using gridding [computerised tomography application]. IEEE transactions on medical imaging. 1991; 10:473–478. [PubMed: 18222850]

Kahn I, Knoblich U, Desai M, Bernstein J, Graybiel AM, Boyden ES, Buckner RL, Moore CI. Optogenetic drive of neocortical pyramidal neurons generates fMRI signals that are correlated with spiking activity. Brain research. 2013; 1511:33–45. [PubMed: 23523914]

Kilner JM, Mattout J, Henson R, Friston KJ. Hemodynamic correlates of EEG: a heuristic. Neuroimage. 2005; 28:280–286. [PubMed: 16023377]

Kim DH, Adalsteinsson E, Spielman DM. Simple analytic variable density spiral design. Magnetic resonance in medicine. 2003; 50:214–219. [PubMed: 12815699]

Kravitz AV, Freeze BS, Parker PR, Kay K, Thwin MT, Deisseroth K, Kreitzer AC. Regulation of parkinsonian motor behaviours by optogenetic control of basal ganglia circuitry. Nature. 2010; 466:622–626. [PubMed: 20613723]

Kuhn AA, Kempf F, Brucke C, Gaynor Doyle L, Martinez-Torres I, Pogosyan A, Trottenberg T, Kupsch A, Schneider GH, Hariz MI, et al. High-frequency stimulation of the subthalamic nucleus suppresses oscillatory beta activity in patients with Parkinson's disease in parallel with improvement in motor performance. The Journal of neuroscience : the official journal of the Society for Neuroscience. 2008; 28:6165–6173. [PubMed: 18550758]

Kuhn AA, Tsui A, Aziz T, Ray N, Brucke C, Kupsch A, Schneider GH, Brown P. Pathological synchronisation in the subthalamic nucleus of patients with Parkinson's disease relates to both bradykinesia and rigidity. Experimental neurology. 2009; 215:380–387. [PubMed: 19070616]

Lee HJ, Weitz AJ, Bernal-Casas D, Duffy BA, Choy M, Kravitz AV, Kreitzer AC, Lee JH. Activation of direct and indirect pathway medium spiny neurons drives distinct brain-wide responses. Neuron. 2016; 9:412–424.

Lee JH, Durand R, Gradinaru V, Zhang F, Goshen I, Kim DS, Fenno LE, Ramakrishnan C, Deisseroth K. Global and local fMRI signals driven by neurons defined optogenetically by type and wiring. Nature. 2010; 465:788–792. [PubMed: 20473285]

Levy R, Ashby P, Hutchison WD, Lang AE, Lozano AM, Dostrovsky JO. Dependence of subthalamic nucleus oscillations on movement and dopamine in Parkinson's disease. Brain : a journal of neurology. 2002; 125:1196–1209. [PubMed: 12023310]

Li B, Daunizeau J, Stephan KE, Penny W, Hu D, Friston K. Generalised filtering and stochastic DCM for fMRI. Neuroimage. 2011; 58:442–457. [PubMed: 21310247]

Liu J, Lee HJ, Weitz AJ, Fang Z, Lin P, Choy M, Fisher R, Pinskiy V, Tolpygo A, Mitra P, et al. Frequency-selective control of cortical and subcortical networks by central thalamus. eLife. 2015; 4:e09215. [PubMed: 26652162]

Logothetis NK. What we can do and what we cannot do with fMRI. Nature. 2008; 453:869–878. [PubMed: 18548064]

Magill PJ, Bolam JP, Bevan MD. Dopamine regulates the impact of the cerebral cortex on the subthalamic nucleus-globus pallidus network. Neuroscience. 2001; 106:313–330. [PubMed: 11566503]

McIntyre CC, Savasta M, Kerkerian-Le Goff L, Vitek JL. Uncovering the mechanism(s) of action of deep brain stimulation: activation, inhibition, or both. Clinical neurophysiology : official journal of the International Federation of Clinical Neurophysiology. 2004; 115:1239–1248. [PubMed: 15134690]

Nini A, Feingold A, Slovin H, Bergman H. Neurons in the globus pallidus do not show correlated activity in the normal monkey, but phase-locked oscillations appear in the MPTP model of parkinsonism. Journal of neurophysiology. 1995; 74:1800–1805. [PubMed: 8989416]

Ohayon S, Grimaldi P, Schweers N, Tsao DY. Saccade modulation by optical and electrical stimulation in the macaque frontal eye field. The Journal of neuroscience : the official journal of the Society for Neuroscience. 2013; 33:16684–16697. [PubMed: 24133271]

Ourselin S, Roche A, Subsol G, Pennec X, Ayache N. Reconstructing a 3D structure from serial histological sections. Image Vision Comput. 2001; 19:25–31.

Paxinos, G., Franklin, KB. The mouse brain in stereotaxic coordinates. Vol. 2. Academic; San Diego: 2001.

Payoux P, Remy P, Damier P, Miloudi M, Loubinoux I, Pidoux B, Gaura V, Rascol O, Samson Y, Agid Y. Subthalamic nucleus stimulation reduces abnormal motor cortical overactivity in Parkinson disease. Archives of neurology. 2004; 61:1307–1313. [PubMed: 15313852]

Penny WD, Stephan KE, Daunizeau J, Rosa MJ, Friston KJ, Schofield TM, Leff AP. Comparing families of dynamic causal models. PLoS Comput Biol. 2010; 6:e1000709. [PubMed: 20300649]

Penny WD, Stephan KE, Mechelli A, Friston KJ. Comparing dynamic causal models. Neuroimage. 2004; 22:1157–1172. [PubMed: 15219588]

Priori A, Foffani G, Pesenti A, Tamma F, Bianchi AM, Pellegrini M, Locatelli M, Moxon KA, Villani RM. Rhythm-specific pharmacological modulation of subthalamic activity in Parkinson's disease. Experimental neurology. 2004; 189:369–379. [PubMed: 15380487]

Priori A, Lefaucheur JP. Chronic epidural motor cortical stimulation for movement disorders. The Lancet Neurology. 2007; 6:279–286. [PubMed: 17303534]

Razi A, Kahan J, Rees G, Friston KJ. Construct validation of a DCM for resting state fMRI. Neuroimage. 2015; 106:1–14. [PubMed: 25463471]

Ridding MC, Inzelberg R, Rothwell JC. Changes in excitability of motor cortical circuitry in patients with Parkinson's disease. Annals of neurology. 1995; 37:181–188. [PubMed: 7847860]

Schroll H, Hamker FH. Computational models of basal-ganglia pathway functions: focus on functional neuroanatomy. Frontiers in systems neuroscience. 2013; 7:122. [PubMed: 24416002]

Sporns, O. Networks of the Brain. The MIT Press; 2010.

Stephan KE, Kasper L, Harrison LM, Daunizeau J, den Ouden HE, Breakspear M, Friston KJ. Nonlinear dynamic causal models for fMRI. Neuroimage. 2008; 42:649–662. [PubMed: 18565765]

Stephan KE, Penny WD, Daunizeau J, Moran RJ, Friston KJ. Bayesian model selection for group studies. Neuroimage. 2009; 46:1004–1017. [PubMed: 19306932]

Walker HC, Watts RL, Guthrie S, Wang D, Guthrie BL. Bilateral effects of unilateral subthalamic deep brain stimulation on Parkinson's disease at 1 year. Neurosurgery. 2009; 65:302–309. discussion 309-310. [PubMed: 19625909]

Wang L, Saalmann YB, Pinsk MA, Arcaro MJ, Kastner S. Electrophysiological low-frequency coherence and cross-frequency coupling contribute to BOLD connectivity. Neuron. 2012; 76:1010–1020. [PubMed: 23217748]

Weinberger M, Hutchison WD, Dostrovsky JO. Pathological subthalamic nucleus oscillations in PD: can they be the cause of bradykinesia and akinesia? Experimental neurology. 2009; 219:58–61. [PubMed: 19460368]

Weitz AJ, Fang Z, Lee HJ, Fisher RS, Smith WC, Choy M, Liu J, Lin P, Rosenberg M, Lee JH. Optogenetic fMRI reveals distinct, frequency-dependent networks recruited by dorsal and intermediate hippocampus stimulations. Neuroimage. 2015; 107:229–241. [PubMed: 25462689]

Weitz AJ, Lee JH. Progress with optogenetic functional MRI and its translational implications. Future Neurology. 2013; 8:691–700.

Whitmer D, de Solages C, Hill B, Yu H, Henderson JM, Bronte-Stewart H. High frequency deep brain stimulation attenuates subthalamic and cortical rhythms in Parkinson's disease. Frontiers in human neuroscience. 2012; 6:155. [PubMed: 22675296]

Wingeier B, Tcheng T, Koop MM, Hill BC, Heit G, Bronte-Stewart HM. Intra-operative STN DBS attenuates the prominent beta rhythm in the STN in Parkinson's disease. Experimental neurology. 2006; 197:244–251. [PubMed: 16289053]

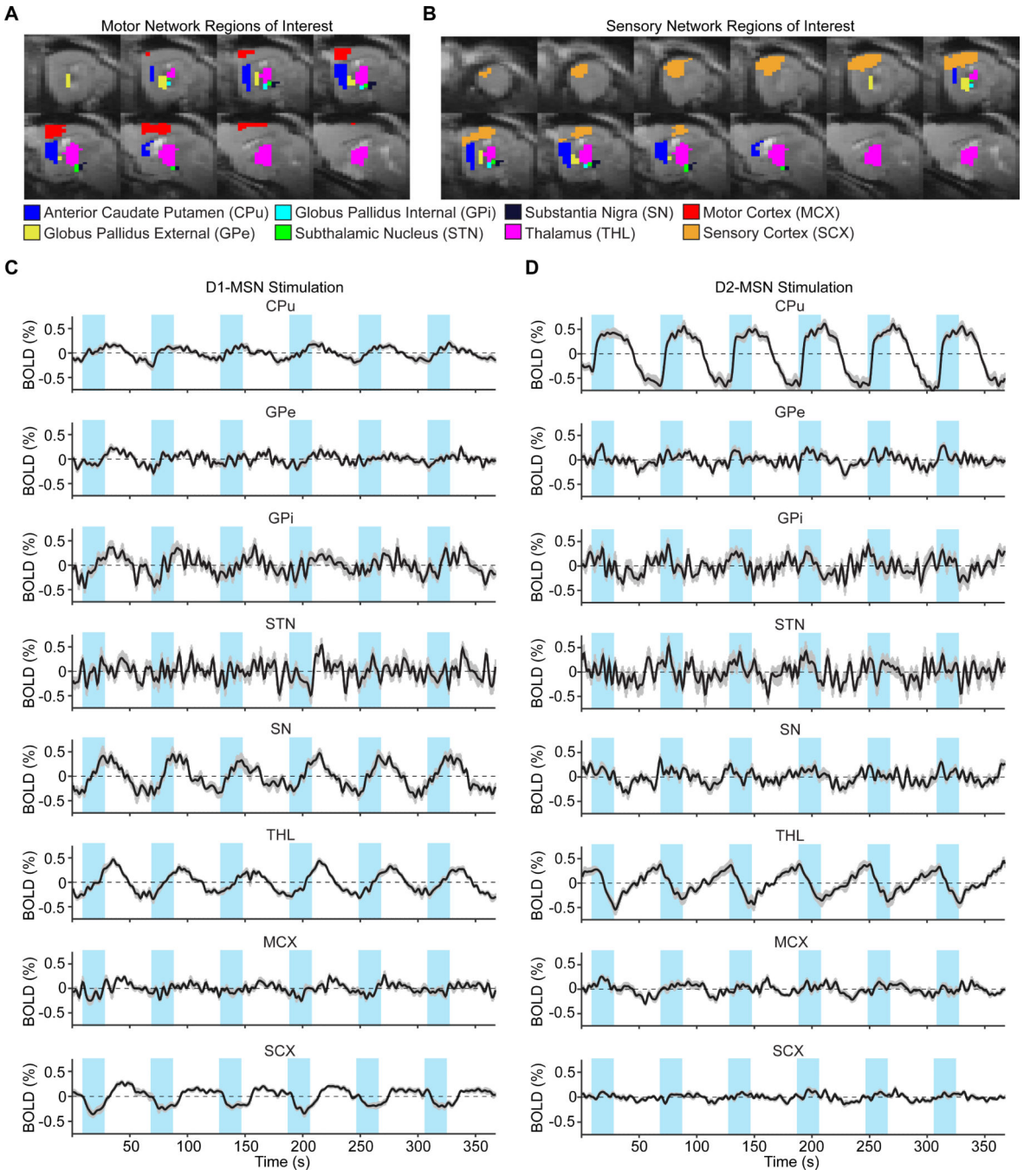

Figure 1. Anatomical masks and time series extracted from regions of interest (ROIs) within the basal ganglia-thalamocortical network

A,B, Anatomical masks for time series extraction and model estimation of the MCX and SCX network models, respectively. **C,D**, Time series extracted from ROIs of the left (ipsi-stimulation) hemisphere during D1- and D2-MSN stimulations, respectively. Time series are zero-mean, and represent average signal changes across all voxels and subjects (D1-MSN stimulation: $n = 12$, D2-MSN stimulation: n = 11). Error bars represent the standard error of the mean activation values across subjects. The blue rectangles overlying time series here

and in all future panels represent the 20 s periods of optogenetic activation, delivered every minute for six minutes.

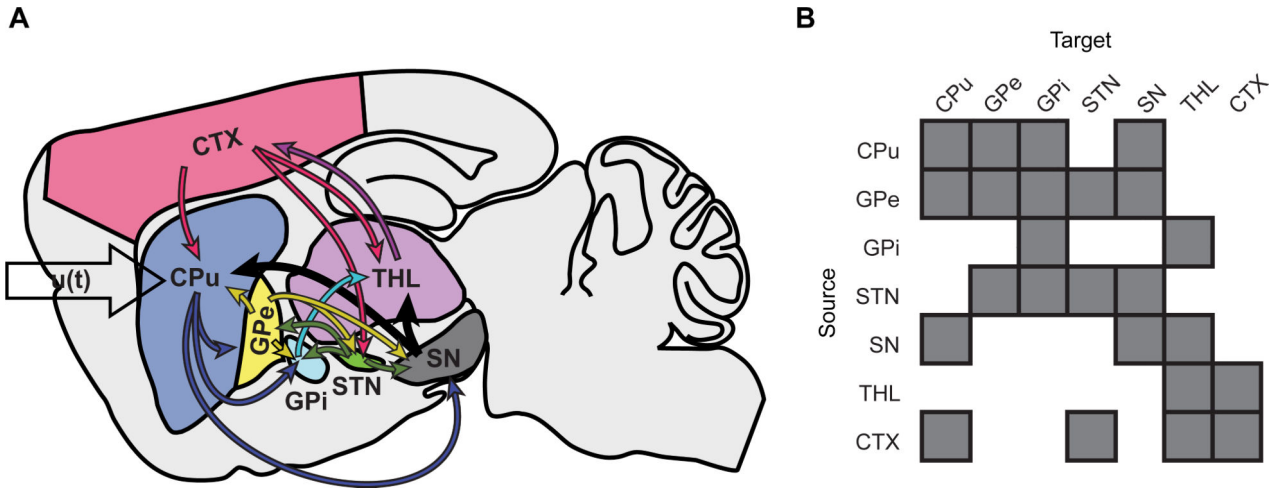

Figure 2. Basal ganglia-thalamocortical network model

A, Schematic representation of the *a priori* generative network model employed in this study. *u(t)* denotes input to the CPu network node modeling optogenetic stimulation. **B**, Graphical representation of the matrix *A* that describes extrinsic (between region) anatomical connections.

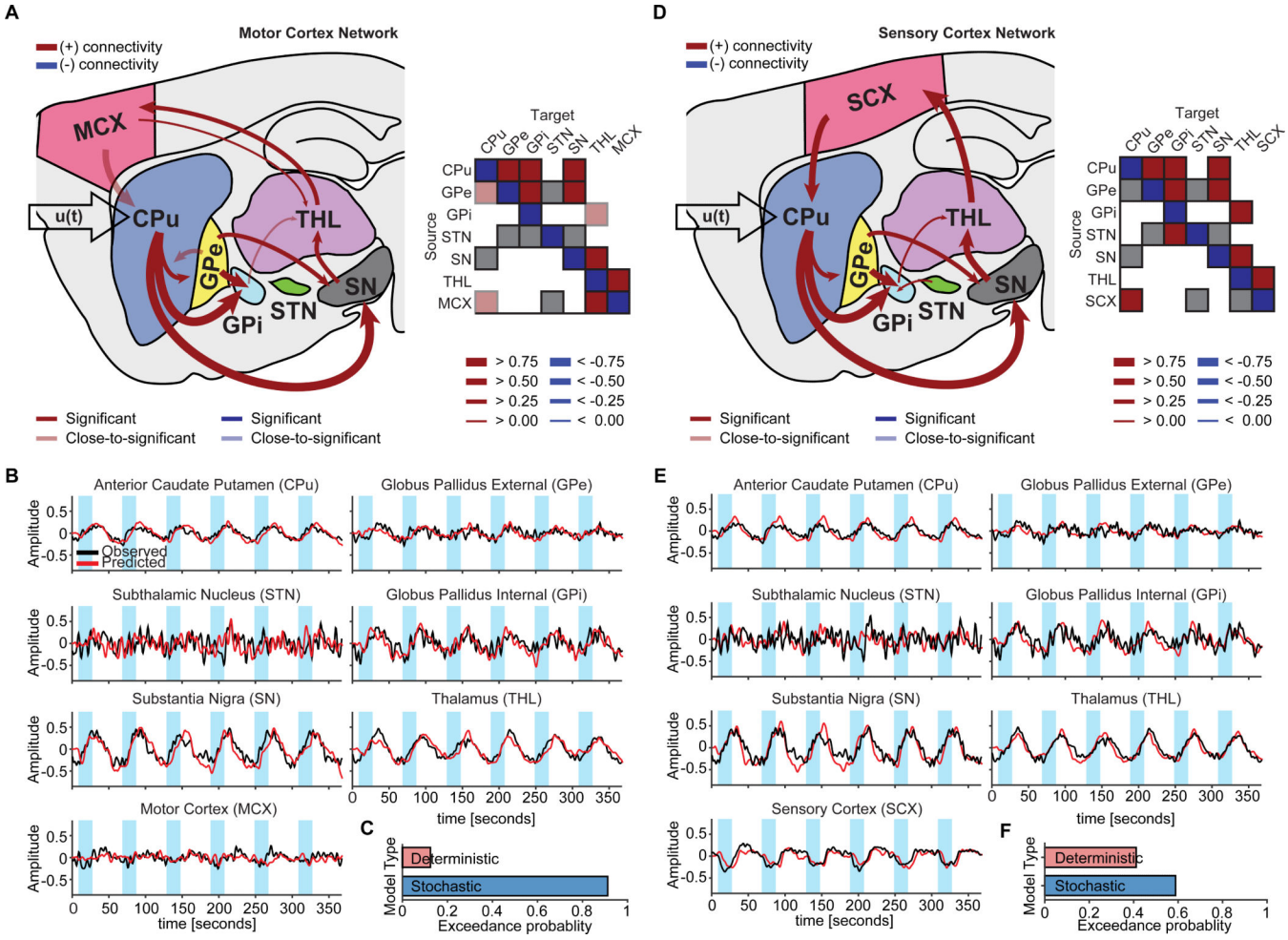

Figure 3. The D1-MSN stimulation network reveals connectivity estimates consistent with the direct pathway

A,D, Significant connections during D1-MSN stimulations for MCX and SCX network models, respectively. The greatest connections for either model were from CPu to GPi and SN, which define the direct pathway. Matrices to the right of each network schematic provide a graphical representation of significant connections. For simplicity, self-connections were not included. **B,E**, Observed and predicted BOLD responses for MCX and SCX network models, respectively. Predicted responses closely fit the observed time series. **C,F**, According to Bayesian model selection, the stochastic modeling fits the observed BOLD responses better than the deterministic modeling for both MCX and SCX networks. Significance levels were corrected for multiple comparisons by means of FDR.

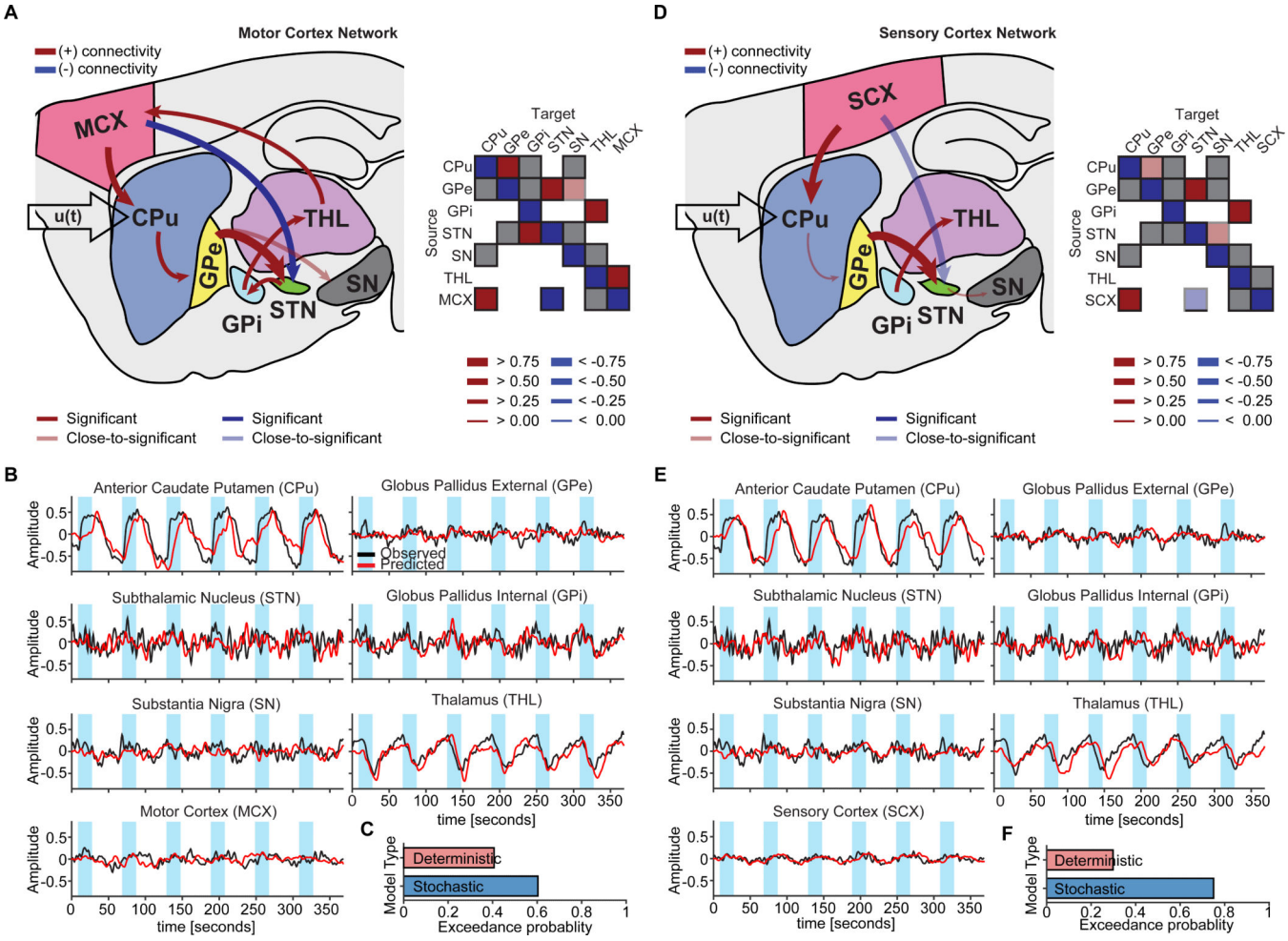

Figure 4. The D2-MSN stimulation network reveals connectivity estimates consistent with the indirect pathway

A,D, Significant connections during D2-MSN stimulations for MCX and SCX network models, respectively. The connection from GPe to STN, which in part defines the indirect pathway, was the greatest connection within either model. Matrices to the right of each network schematic provide a graphical representation of connection strengths. For simplicity, self-connections were not included. **B,E**, Observed and predicted BOLD responses for MCX and SCX network models, respectively. Predicted responses closely fit the observed time series. **C,F**, According to Bayesian model selection, the stochastic modeling fit the observed BOLD responses better than the deterministic modeling in a majority of animals for both MCX and SCX network models. Significance levels were corrected for multiple comparisons by means of FDR.

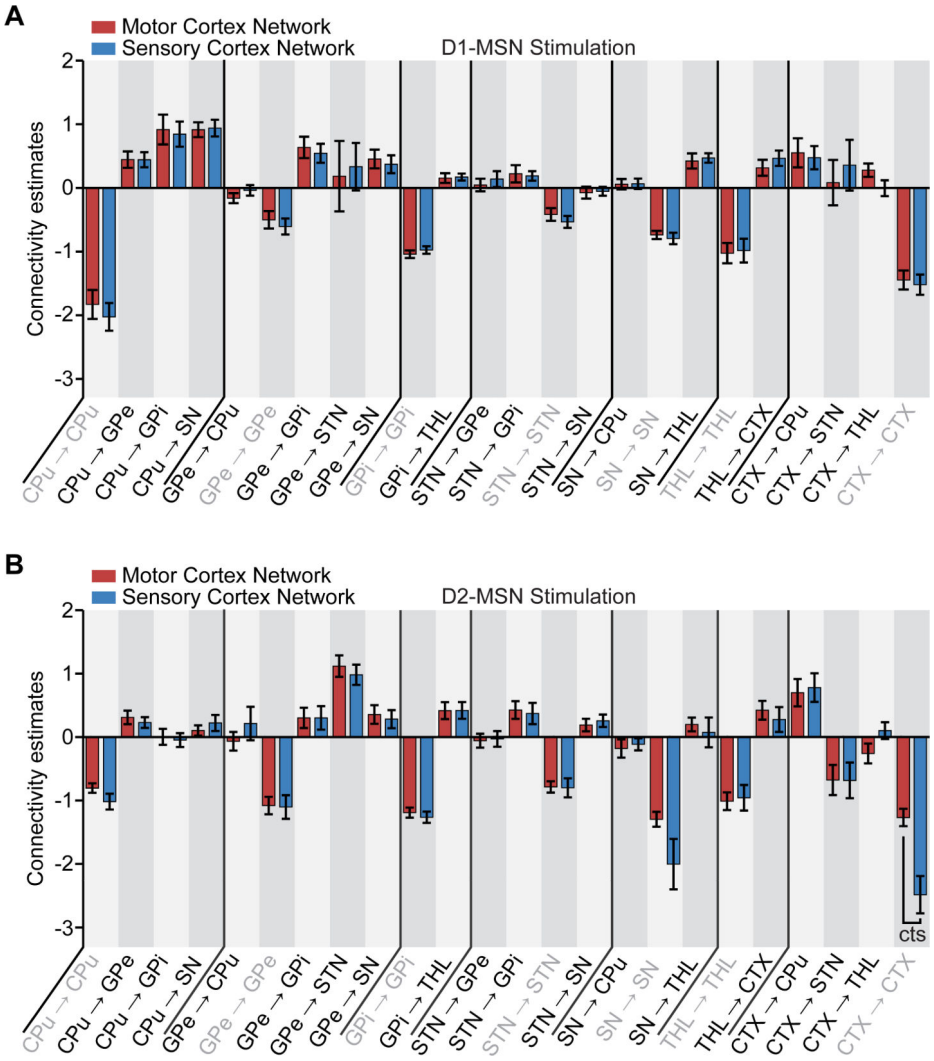

Figure 5. Comparison of connectivity estimates between MCX and SCX network models

A, Comparison of connectivity estimates during D1-MSN stimulations between MCX and SCX network models. No significant differences were observed in the connectivity estimates during D1-MSN stimulations between MCX and SCX network models. **B**, Comparison of connectivity estimates during D2-MSN stimulations between MCX and SCX network models. No differences were observed in the connectivity estimates during D2-MSN stimulations with the exception of the self-connection within CTX. Error bars represent the standard error of the connectivity estimates over subjects. “cts” indicates a close-to-significant difference across subjects after applying a multiple comparison correction across *a priori* connections with FDR ($P < 0.10$).

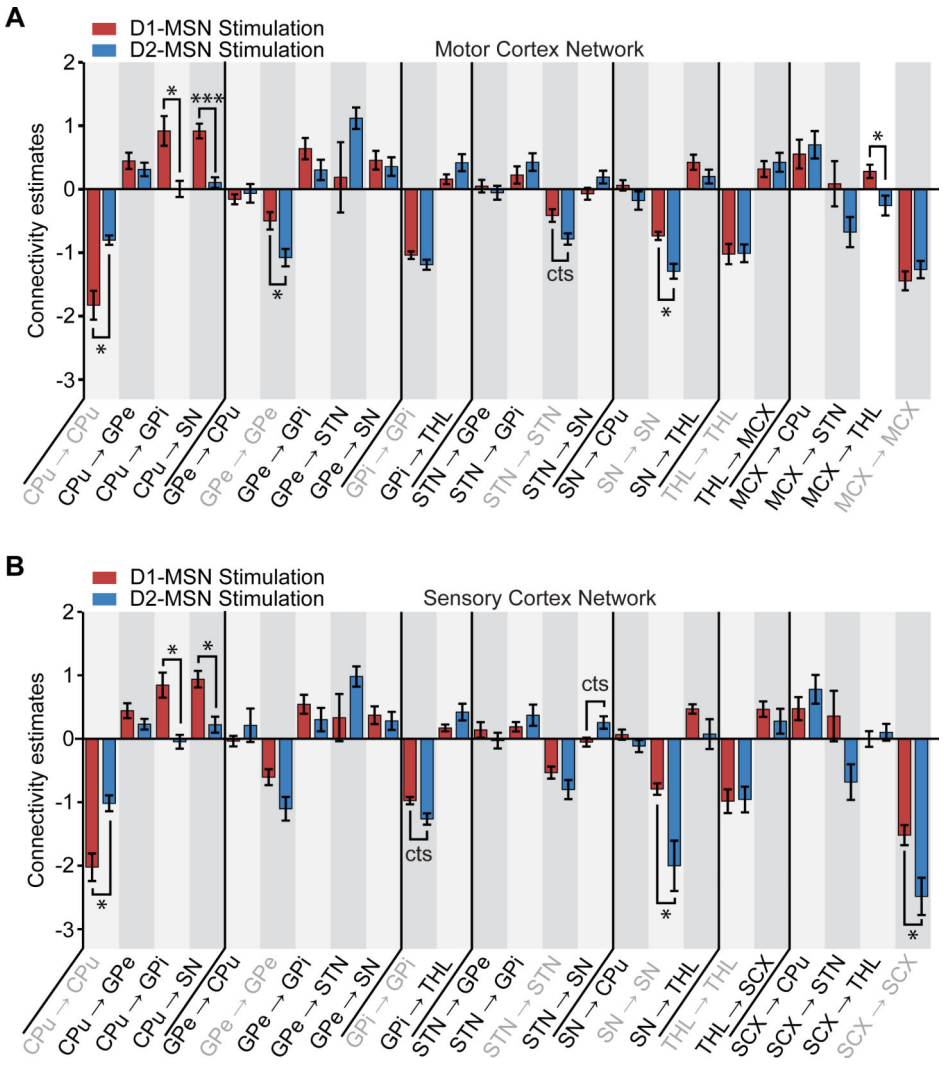

Figure 6. Comparison of connectivity estimates between D1- and D2-MSN stimulation network models

A, Comparison of connectivity estimates between D1- and D2-MSN stimulations for the MCX network model. Statistical differences were observed in the connectivity estimates between D1- and D2-MSN stimulations. **B**, Comparison of connectivity estimates between D1- and D2-MSN stimulations for the SCX network model. Statisticaldifferences were observed in the connectivity estimates between D1- and D2-MSN stimulations. Error bars represent the standard error of the connectivity estimates over subjects. * indicates $P < 0.05$ and *** indicates $P < 0.001$ across subjects after applying a multiple comparison correction across *a priori* connections with FDR; “cts” indicates a close-to-significant difference ($P < 0.10$).